# An Implementation of the Active Contours without Edges model and the Logic Framework for Active contours on multi-channel images

Karim Ali and Sarah Nadi
{karim, snadi}@cs.uwaterloo.ca
David R. Cheriton School of Computer Science
University of Waterloo

## Abstract

*In this project, we provide an implementation for the Chan-Vese model for active contours without edges, and the Sandberg-Chan logic framework for active contours on multi-channel images. The Chan-Vese model is a special case of the more general Mumford-Shah functional for segmentation and level sets. It differs from other active contour models in that it does not depend on the gradient of the contour ($\phi$), therefore it is more capable of detecting objects whose boundaries may not be defined by a gradient (e.g. blurry images, noisy images). The Sandberg-Chan model builds on top of the Chan-Vese model by allowing the contour to evolve simultaneously on multiple channels. It also offers a set of logic operations that can be applied to those channels (union, intersection, complement, and their combinations). We evaluate our implementation based on several criteria, such as: independence of initial curve position, successful detection of holes, performance with blurred and noisy images, and response to scaling parameters.*

## 1. Introduction

Image segmentation or boundary detection is a very important problem in the area of Image Processing, and has received a lot of attention in the past. The classical Active Contour model (or Snakes) proposed by Kass et al. [3] was the first model to use the idea of energy minimization to attract a contour to the edges of the objects in an image. The Snakes model was very successful and variations of it very highly adopted later on (E.g. [1]. Most of these models used the level set formulation for propagating fronts to evolve the curve. However, these models highly depended on curvature motion (motion defined by the gradient of the curve) which led to poor performance in smoothed edges. To overcome these limitations, Chan and Vese [2] propose an active contour model that does not depend on the edges (i.e the gradient) for propagating the curve to detect the boundary of the object. Instead, they use a region-based approach based on the Mumford-Shah model [4] to divide the image into two regions: one inside the propagating curve, and one outside. The curve is at the boundary of the object if there is no difference in intensities inside the curve as well as outside the curve.

The Active Contours without Edges model proposed by Chan and Vese (referred to as Chan-Vese model throughout the rest of this paper) was very successful in detecting objects even in noisy or blurry images. It could also detect holes in objects which was usually a limitation in previous models. As an extension to this work, Sandberg and Chan [5] propose a logic framework (referred to as the Sandberg-Chan model throughout the rest of this paper) that performs logical operations on multiple images according to the curve propagation proposed in the Chan-Vese model. To achieve that, previous models usually had two steps. They would either first segment the object in each channel separately then combine the segmented objects according to the logic operation through bitwise operations (E.g. [6, 7]) or they would apply logic operations to the different images then segment the resulting image. The first approach is very costly, and the second approach requires a lot of prior knowledge about the intensities of each image. To overcome these drawbacks, the Sandberg-Chan model is based on the idea of fitting a single contour to the object on all channels according to the logic operator, and based on regions.

In this paper, we report on our findings after implementing each of these models. We implemented both models in Matlab, and experimented with several images. In this paper, we explain the details of our implementation as well as our results. The rest of this paper is organized as follows: Section 2 first provides brief background about each of the two models implemented in this paper. Section 3 then explains our implementation. In this section, we explain how we implemented the models and any variations from the original papers. Section 4 explains our evalua-

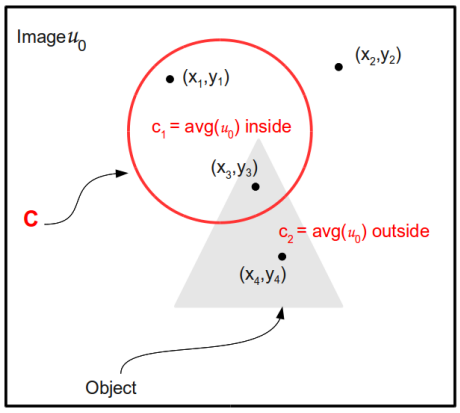


Figure 1. Region Based Model

tion criteria, and presents the results we obtained. Section 5 discusses some of the difficulties we faced, and points out some BLA. Section 6 concludes this paper by summarizing our findings.

## 2. Background

### 2.1. Chan-Vese Model

The Chan-Vese model is a region based model for detecting objects in an image. It is based on a restriction Mumford-Shah model which divides an image into regions and represents each region by a piecewise constant (the minimal partition problem). Figure 1 shows what is meant by a region based model. The figure shows an image $u_0$ which has a gray triangular object in it. The red curve, C, is the initial contour used to detect this object. The main idea behind the model is that the curve divides the image into two regions: that inside the curve and that outside. Each region is represented by a constant, c, which is the average intensity of the image values in each region. In order for the curve to fit the object, there must be no variation of the intensities inside the curve as well as outside. In other words, this turns into a minimization problem of the difference of intensities inside (fitting term one, $F_1$) plus those outside (fitting term two, $F_2$). For example, in the figure, the point $(x_1, y_1)$ will have to be outside the curve in order to minimize the difference between the points inside the curve. Similarly, the point $(x_4, y_4)$ will have to be inside the curve. Figure 2 shows all the possibilities of the curve's fitting according to its position with respect to the object.

More formally, the Euler-Lagrange equation (as derived in the original paper) representing the time motion of the curve C is shown in Equation 1.

$$\frac{\partial \phi}{\partial t} = \delta_\varepsilon(\phi)[\mu \ \mathrm{div}(\frac{\bigtriangledown \phi}{|\bigtriangledown \phi|}) - \nu - \lambda_1(u_0 - c_1)^2 + \lambda_2(u_0 - c_2)^2] \quad (1)$$

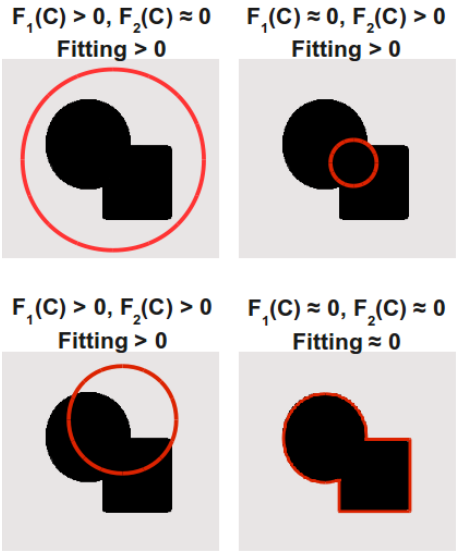


Figure 2. Chan-Vese Curve Fitting

The parameter $\mu$ is a scaling parameter for the length of the curve represented in terms of curvature. The smalled $\mu$ is, the more the length of the curve can increase without penalizing the minimization. This allows the model to detect smalled objects and holes. The larger $\mu$ is, the less freedom there is for the curve to increase in length, and thus, it will only be able to detect larger objects. The parameter $\nu$ is also a scaling term for the area of the curve. However, the authors do not use the area term in the Euler-Lagrange derivation, and always set $\nu$ to 0. It seems that $\mu$ is sufficient to scale the curve according to the objects that need to be detected. Finally, $\lambda_1$ and $\lambda_2$ are weighting parameters for the forces inside the curve and outside the curve respectively. Since we want to give both forces equal weight, the authors set $\lambda_1 = \lambda_2 = 1$ in all their experiments.

### 2.2. Sandberg-Chan Model

The main goal of the Sandberg-Chan model [5] is to perform logic operations on a combination of different images accurately and efficiently. For example, finding the union of two images where different parts of the object are occluded in each image so that a complete object can be obtained. In order to do that, they use the Chan-Vese model to detect objects, and simultaneously include the logic operations in the minimization problem. Since they are using the Chan-Vese model, the problem must be viewed in terms of regions as well. Accordingly, they define the two main logic operations (union and intersection) in terms of regions where the union of two images is the union of the insides of the curve with respect to the images plus the intersection of the outsides of the curve with respect to the images. For example, Figure 3 (taken from the original paper) shows that the union of $A_1$ and $A_2$ (in terms of its shape) can be ob-

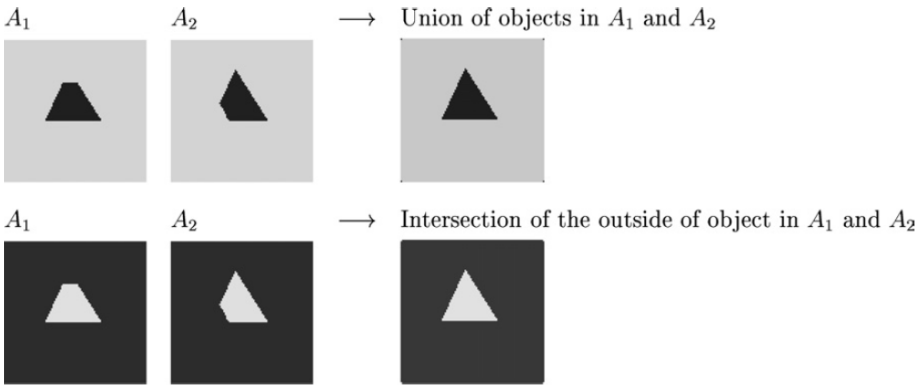


Figure 3. Region Based View Union

tained by taking the union of the insides of the object or the intersection of the outsides. Similarly, the intersection of two images would be the intersection of the insides plus the union of the outsides. Thus, in order to obtain accurate results irrespective of the object's intensity outside versus inside, we should consider *both* the logical operation required for the region inside the object as well as that outside.

More formally, the authors define two logic variables $z_i^{in}$ and $z_i^{out}$ to denote whether a point $(x, y)$ should be in the moving curve C or not with respect to image i. Since we are trying to minimize the fitting of the curve, they use 0 to denote true and 1 to denote false (the reverse of the usual convention. Following the Chan-Vese model, they represent each of the regions inside and outside the curve by a constant c. In this paper, they represent $c_{in}$ as $c_+$ and $c_{out}$ as $c_-$. Equations 2 and 3 show how to calculate $z_{in}$ and $z_{out}$ respectively in terms of the Chan-Vese model. We note here that in the original paper there was a typo in these equations where they divide by the maximum intensity of each image instead of the maximum intensity squared. However, in order to have $z_{in}$ and $z_{out}$ have values from 0 to 1 that represent logic values, we need to divide by the maximum intensity squared. The equations shown below have been corrected for that.

$$z_i^{in}(u_0^i, x, y, C) = \frac{|u_0^i - c_+^i|^2}{(max_{(x,y)\in u_0^i} u_0^i)^2} \tag{2}$$

$$z_i^{out}(u_0^i, x, y, C) = \frac{|u_0^i - c_-^i|^2}{(max_{(x,y)\in u_0^i} u_0^i)^2} \tag{3}$$

In order to perform logic operations on $z_{in}$ and $z_{out}$, the authors introduce interpolation functions that mimic the behavior of the regular truth table, but for continuous values between 0 and 1. The union and intersection functions for two variables are shown in Equations 4 and 5 respectively. These equations can be simply extended to any number of variables.

$$f_\cup = (z_1.z_2)^{1/2} \tag{4}$$

$$f_\cap = 1 = ((1 - z_1).(1 - z_2))^{1/2} \tag{5}$$

Based on these functions, the Euler-Lagrange equation for any logic operation is shown in Equation 6. According to the desired logic operation, $f_{in}$ and $f_{out}$ will be specified accordingly. For example, if we are doing the union of the images, then we will need to perform a union operation on the insides. Thus, $f_{in}$ will be replaced by Equation 4. Similarly, we will need to do the intersection of the outsides so $f_{out}$ will be replaced by Equation 5.

$$\frac{\partial \phi}{\partial t} = \delta(\phi)[\mu \bigtriangledown (\frac{\bigtriangledown \phi}{|\bigtriangledown \phi|}) - \lambda(f_{in}(z_1^{in}, ..., z_n^{in}) - f_{out}(z_1^{out}, ..., z_n^{out}) \tag{6}$$

## 3. Implementation

During implementation, we tried to stick to the authors' formulas and guidelines as much as possible. In this section we explain the choices we made regardless implementation. For the chan-vese model, we used the PDE given in Equation 9 in the original paper [2] which is shown in Equation 1. We, first, tried to implement the delta dirac function, $\delta_\varepsilon \phi$, as defined in the paper. However, we did not get non-zero values everywhere as indicated by the authors. Accordingly, we chose to use $|\bigtriangledown \phi|$ instead of the delta dirac function as this was indicated as a valid alternative by the authors. To calculate $c_1$ and $c_2$, we simply calculated the mean of the values inside $\phi$ (specifically where $\phi > 0$) and the mean of the values outside $\phi$ (specifically where $\phi < 0$) respectively. To actually solve the PDE, we chose to use an explicit time stepping scheme for the finite difference discretization. That is, in each time step $\phi_t = \phi + \triangle t * force$. This was simpler to implement, and although $\triangle t$ must be chosen carefully to satisfy the stability condition, we did not suffer from performance problems due to this restriction.

| Criteria | Goal | Applies to Model |
|---|---|---|
| Detecting Boundaries | Ability to correctly detect object boundaries of simple objects | Both Models |
| Curve Position | Ability to correctly detect object boundaries irrespective of the initial curve position | Both Models |
| Detecting Holes | Ability to detect holes in objects, and not simply stop on outside boundary | Both Models |
| Blurred Images | Ability to correctly (as much as possible) detect object boundaries in blurred images | Both Models |
| Noisy Images | Ability to correctly (as much as possible) detect object boundaries in noisy images | Both Models |
| Union Operator | Ability to correctly obtain the union of two or more images | Sandberg-Chan |
| Intersection Operator | Ability to correctly obtain the intersection of two or more images | Sandberg-Chan |
| Complement | Ability to correctly obtain the union or intersection of two or more images containing complements | Sandberg-Chan |
| Parameter Settings | Ability to respond correctly to the different parameter settings | Both Models |

Table 1. Evaluation Criteria

For the sandberg-chan model, we used the PDE given in original paper as well, and shown in Equation 6. Again, we used $|\bigtriangledown \phi|$ instead of the dirac function. We calculated $z_{in}$ and $z_{out}$ according to Equations **??** shown above which have been corrected for the typo in the original paper. For all other equations and calculations necessary in the model, we closely followed the original paper in our implementation. We also used an explicit time stepping scheme in this model.

## 4. Experimental Results

In order to make sure we correctly implemented the models, we had several evaluation criteria. Table 1 summarizes these criteria, and explains the goals of each. Some of these criteria apply for both models, while other apply to one or the other. For the rest of this section, we proceed by presenting our experimental results for both models. For each model, we proceed in the order of these criteria starting with the simplest cases, and incrementally challenging the model. Unless otherwise stated, all the segmentation was performed on a gray scale version of the original image. All the images in the Chan-Vese model were run on a BLA COMPUTER and all the images in the Sandberg-Chan model were run on a BLA computer. As shown in the results, we tried different image sizes to ensure that our solution converges.

### 4.1. Chan-Vese Model Results

We present the results from the Chan-Vese model in this section, and show which criteria were met and which were not. Unless otherwise specified, we set $\lambda_1 = \lambda_2 = 1$.

#### Successful Detection of Boundaries

Figure 4 shows that the implemented model can successfully detect object boundaries in a simple image. In this case, the evolving curve was successfully able to detect the boundaries of both objects. Figure 5 shows a slightly more complicated example where the evolving contour successfully detects the contour of the brain. Note that there is a tiny area to the bottom left of the brain that was also successfully detected. To ensure that open boundaries (e.g. lines) can also be detected, we used an image with several shapes shown in Figure 6;

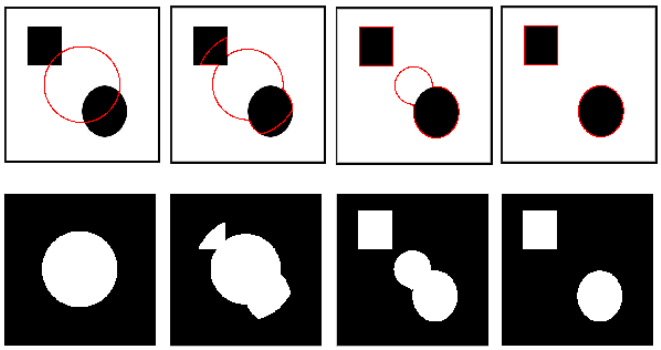

Figure 4. Successful detection of object boundaries. Top: the evolving curve (in red) over time where the first image shows the initial contour. Bottom: evolving segmentation over time until the objects are detected. Size = 300 x 300, $\phi_0(x,y) = -\sqrt{(x-150)^2+(y-150)^2)} + 75$, $\mu = 0.01$, no reinitialization, cpu = 2.9s, 7 iterations.

#### Independence of Initial Curve Position

To ensure that the position of the curve does not affect the final segmentation, we tested two other positions for the initial curve for the lesame brain image used in Figure 5. In Figure 5, the initial contour was completely overlapping the object. Accordingly, we tried two other positions. The first one is shown in Figure 7 where the initial contour only partially overlaps with the object. The second one is shown in Figure 8 where the initial contour does not overlap the object in any part. Visually, the obtained segmentation was the same with a slightly higher number of iterations and CPU time. In all three cases, the brain was correctly segmented. We compared the area segmented as the brain in each case to make sure the same segmentation was obtained, and in each case, we got the same area of 0.5268. Note, however, that when part of the curve lies outside the object, the definition of inside and outside changes since the curve becomes an open curve at one point. This should not make a difference as long as the contour lies correctly at the boundaries

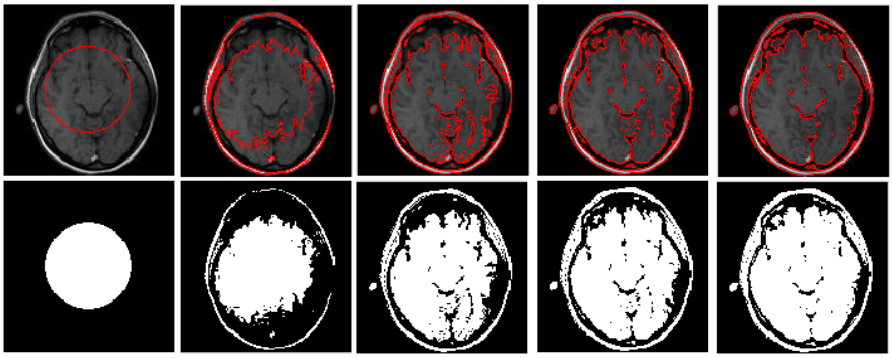

Figure 5. Successful detection of object boundaries. Top: the evolving curve (in red) over time where the first image shows the initial contour. Bottom: evolving segmentation over time until the object is detected. Size = 131 x 131, $\phi_0(x, y) = -\sqrt{(x - 65.6)^2 + (y - 65.5)^2)} + 32.8$, $\mu = 0.01$, no reinitialization, cpu = 1.95 s, took 7 iterations.

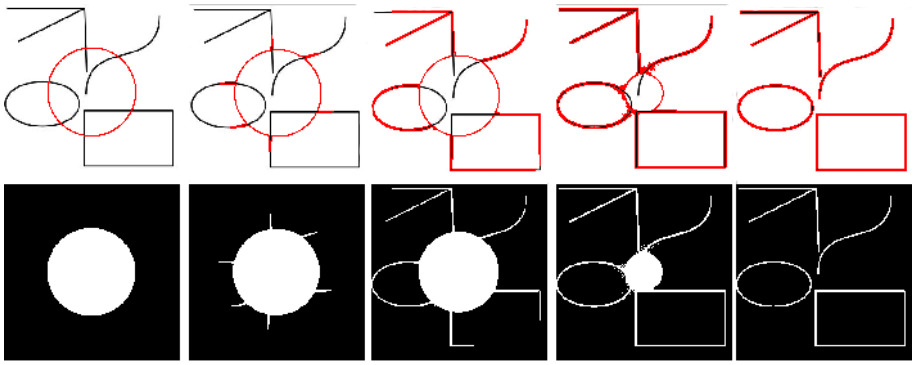

Figure 6. Successful detection of object with open boundaries. Top: the evolving curve (in red) over time where the first image shows the initial contour. Bottom: evolving segmentation over time until the object is detected. Size = 300 x 300, $\phi_0(x, y) = -\sqrt{(x - 150)^2 + (y - 150)^2)} + 75$, $\mu = 0.01$, no reinitialization, cpu = 5.19 s, took 11 iterations.

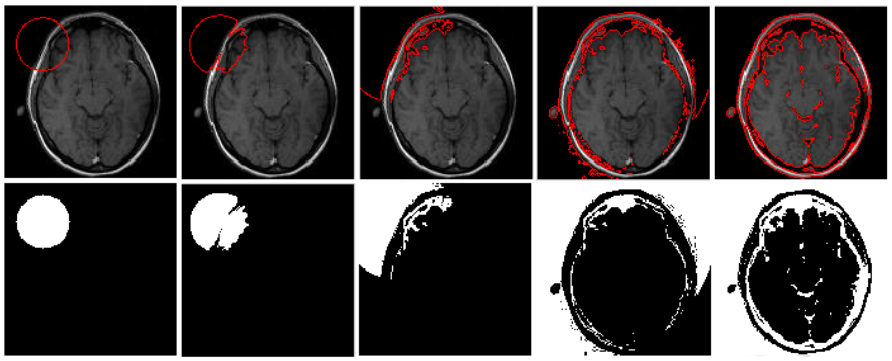

Figure 7. Initial curve position partially overlapping object. Top: the evolving curve (in red) over time where the first image shows the initial contour. Bottom: evolving segmentation over time until the object is detected. Size = 131 x 131, $\phi_0(x, y) = -\sqrt{(x - 30)^2 + (y - 30)^2)} + 20$, $\mu = 0.01$, no reinitialization, cpu = 2.26 s, took 9 iterations.

of the object.

**Successful Detection of Holes**

In order to make sure the contour does not simply stop at the outside boundary of an object and ignore any details inside such as holes, we tried two donut images. Figure 9 shows how the curve is able to detect the hole in the donut. Additionally, it is able to detect the various sprinkles on it. We note that the bottom right boundary is not very exact, and this is because the lighting effect in the image makes the intensity of this area very close to that of the background

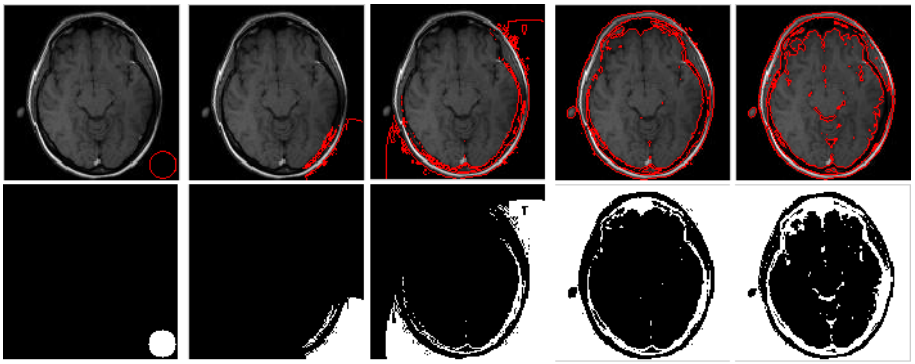

Figure 8. Initial curve position not overlapping any area of the object. Top: the evolving curve (in red) over time where the first image shows the initial contour.Bottom: evolving segmentation over time until the object is detected. Size = 300 x 300, $\phi_0(x,y) = -\sqrt{(x-120)^2+(y-120)^2)}+10$, $\mu = 0.01$, no reinitialization, cpu = 2.01 s, took 9 iterations.

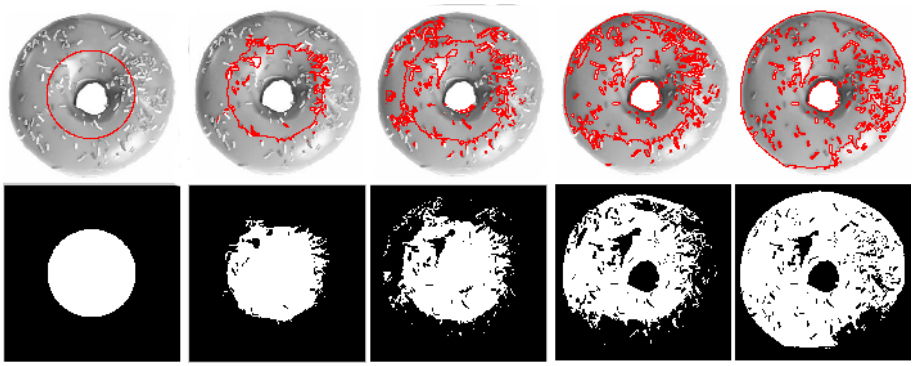

Figure 9. Successful detection of holes. Top: the evolving curve (in red) over time where the first image shows the initial contour.Bottom: evolving segmentation over time until the object is detected. Size = 131 x 131, $\phi_0(x,y) = -\sqrt{(x-65.5)^2+(y-65.5)^2)}+32.8$, $\mu = 0.01$, no reinitialization, cpu = 8.12 s, took 12 iterations.

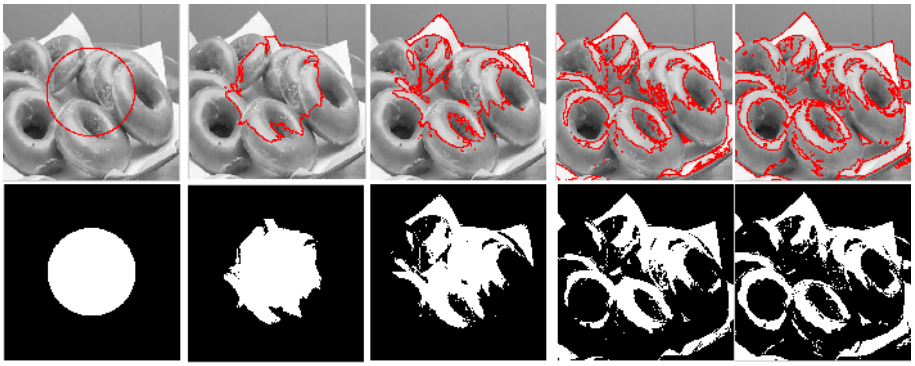

Figure 10. Successful detection of multiple holes. Top: the evolving curve (in red) over time where the first image shows the initial contour.Bottom: evolving segmentation over time until the object is detected. Size = 300 x 300, $\phi_0(x,y) = -\sqrt{(x-150)^2+(y-150)^2)}+75$, $\mu = 0.01$, no reinitialization, cpu = 15.07 s, took 23 iterations.

This is a known drawback of the Chan-Vese model since it only divides the image into two regions, and requires a big variation in intensities for the curve to change. Another example showing this limitation is shown in Figure 11 where the flower parts with very low intensities are not detected. We will show that we can overcome this limitation with the Sandberg-Chan model for this particular example.

Figure 10 shows that multiple holes in an image can also be successfully detected.

### Reasonable Performance with Blurred Images

Figure 12 shows how the contour behaves in a blurry image. The photographer was successfully detected. Additionally,

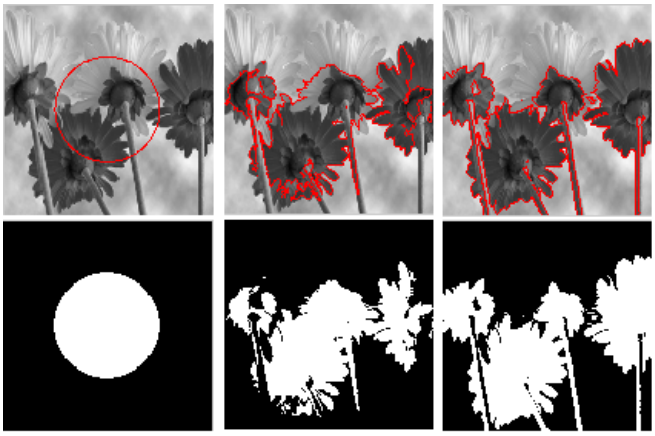

Figure 11. Inability to detect low intensities that have not much variation from their background. Top: the evolving curve (in red) over time where the first image shows the initial contour.Bottom: evolving segmentation over time until the object is detected. Size = 300 x 300, $\phi_0(x,y) = -\sqrt{(x-150)^2+(y-150)^2)}+75$, $\mu = 0.01$, no reinitialization, cpu = 1.35 s, took 6 iterations.

other objects in the image such as the tripod were found. However, objects with a very light intensity were again not detected.

#### Reasonable Performance with Noisy Images

Figure 13 shows how two objects in a noisy image were successfully detected. In this image, we added Gaussian noise with mean zero and 0.01 variance using Matlab's built-in noise function. The image shows that although some of the noise was detected in intermediate iterations, the contour continued to evolve until it was only surrounding the desired objects. Unfortunately, the effect of noise was not completely ignored in all cases. For example, Figure 14 shows that for the same image, but with 'salt & pepper' noise, the noise was detected as objects. This should not have been the case since we used a large value $\mu = 5$ for the length scaling parameter. However, for some reason, varying $\mu$ did not have the intended effect as explained in the next section.

#### Successful Response to Parameter Settings

There are mainly three parameters in this model that can be varied: $\mu, \lambda_1, \lambda_2$. We would usually want both $\lambda_1$ and $\lambda_2$ to be equal to 1 to indicate that we care both about the difference of intensities inside and outside. A smaller weighting for one of them would mean that we would ignore some of the variances in intensities in this area. A larger weighting means that we are magnifying the difference in intensities in that area (i.e. we want to detect any minor changes). We show an example of these variations in Figure 15 where we

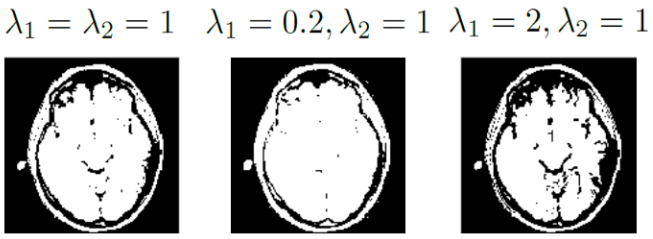


Figure 15. Effect of varying $\lambda_1$ which controls how much details are detected inside the contour. The figure shows the final segmentation in each case.

vary $\lambda_1$ and $\lambda_2$. When we set $\lambda_1 = 0.2$ and $\lambda_2 = 1$, less details within the interior of the brain is detected. When we set $\lambda_1 = 2$ and $\lambda_2 = 1$, we can see that more details within the brain are detected. When we set $\lambda_1 = 5$, and $\lambda_2 = 0.01$ (a very extreme case), we can see that parts of outside boundaries are not well detected, while many details are detected within the brain.

The second parameter, $\mu$ controls how much we allow the length of the curve to increase. If $\mu$ is small, it means that the curve length can increase to detect multiple smaller objects without penalizing our minimization problem. On the other hand if $\mu$ is large, it means that any change in the curve length will be scaled up, and thus will limit the curve expansion to keep the force to a minimum. Unfortunately, we were not able to see this effect in our experiments. We tried varying increasing $\mu$ to be able to detect groupings of objects instead of the individual objects, but the segmentation was invariant to $\mu$. We give more details about how we tried to handle this, and why we believe it is not working in Section 5.

### 4.2. Sandberg-Chan Model Results

For the Sandberg-Chan model, the successful detection of boundaries criteria is implicitly included in the logic operations functionality. We therefore, show the other criteria. Unless otherwise specified, $\mu = 0.1$ and $\lambda = 255 * 255$ in the experiments below.

#### Logic Operators: union and intersection

To ensure that the union operator is working properly, we tried it on a very simple example of two rectangles shown in Figure 16. The union of the two rectangles was successfully detected. Similarly, Figure 17 shows the intersection for the same two simple rectangles.

Figure 18 shows a more complicated example for both the intersection and union with the donut image shown in the previous section. We used two versions of the donuts with each one having a different part occluded. The results of the union and intersection operators are shown in the figure. Additionally, this example shows that the Sandberg-

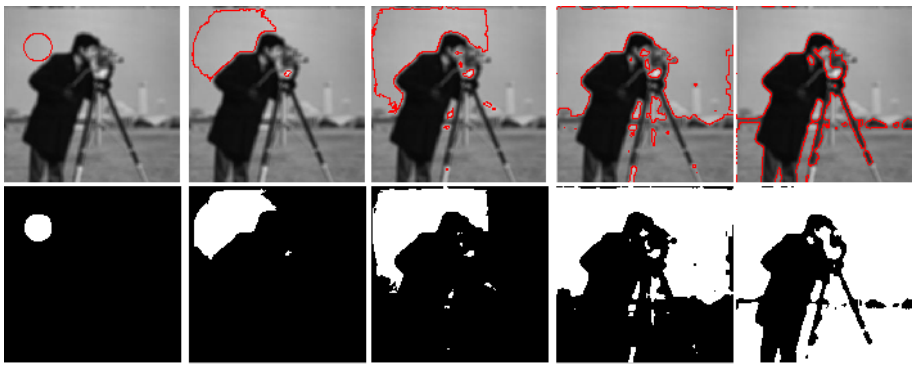

Figure 12. Ability to detect contours in blurry images. Top: the evolving curve (in red) over time where the first image shows the initial contour.Bottom: evolving segmentation over time until the object is detected. Size = 255 x 255, $\phi_0(x, y) = -\sqrt{(x - 127.5)^2 + (y - 127.5)^2)} + 63.75$, $\mu = 0.01$, no reinitialization, cpu = 5.41 s, took 15 iterations.

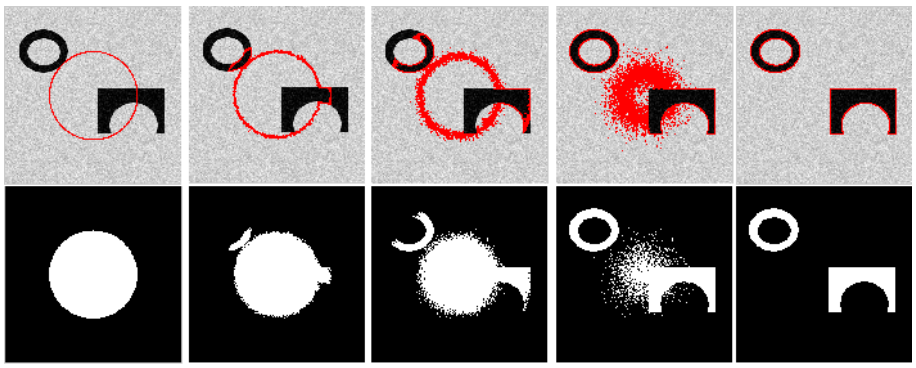

Figure 13. Ability to detect contours in an image with Gaussian noise. Top: the evolving curve (in red) over time where the first image shows the initial contour.Bottom: evolving segmentation over time until the object is detected. Size = 300 x 300, $\phi_0(x, y) = -\sqrt{(x - 150)^2 + (y - 150)^2)} + 75$, $\mu = 0.01$, no reinitialization, cpu = 4.4 s, took 7 iterations.

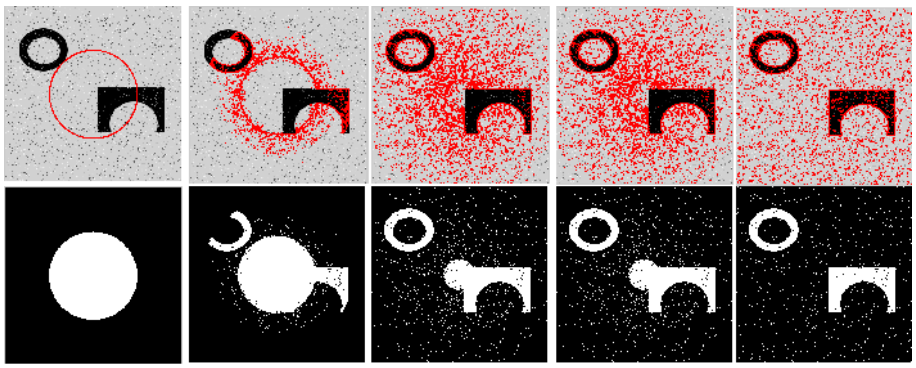

Figure 14. Same image as Figure 13, but with 'salt & pepper' noise. Noise was still detected despite increasing $\mu$. Top: the evolving curve (in red) over time where the first image shows the initial contour.Bottom: evolving segmentation over time until the object is detected. Size = 300 x 300, $\phi_0(x, y) = -\sqrt{(x - 150)^2 + (y - 150)^2)} + 75$, $\mu = 5$, no reinitialization, cpu = 12.27 s, took 7 iterations.

Chan model can still successfully detect holes despite the addition of the logic operations.

A practical usage of this logic operations framework is to recover missing parts from different images, and combine them to produce a more complete image. We show this in Figure 19 which shows two different version of a family image with a child missing in each image. When the union is applied to these two channels, the complete family image is recovered.

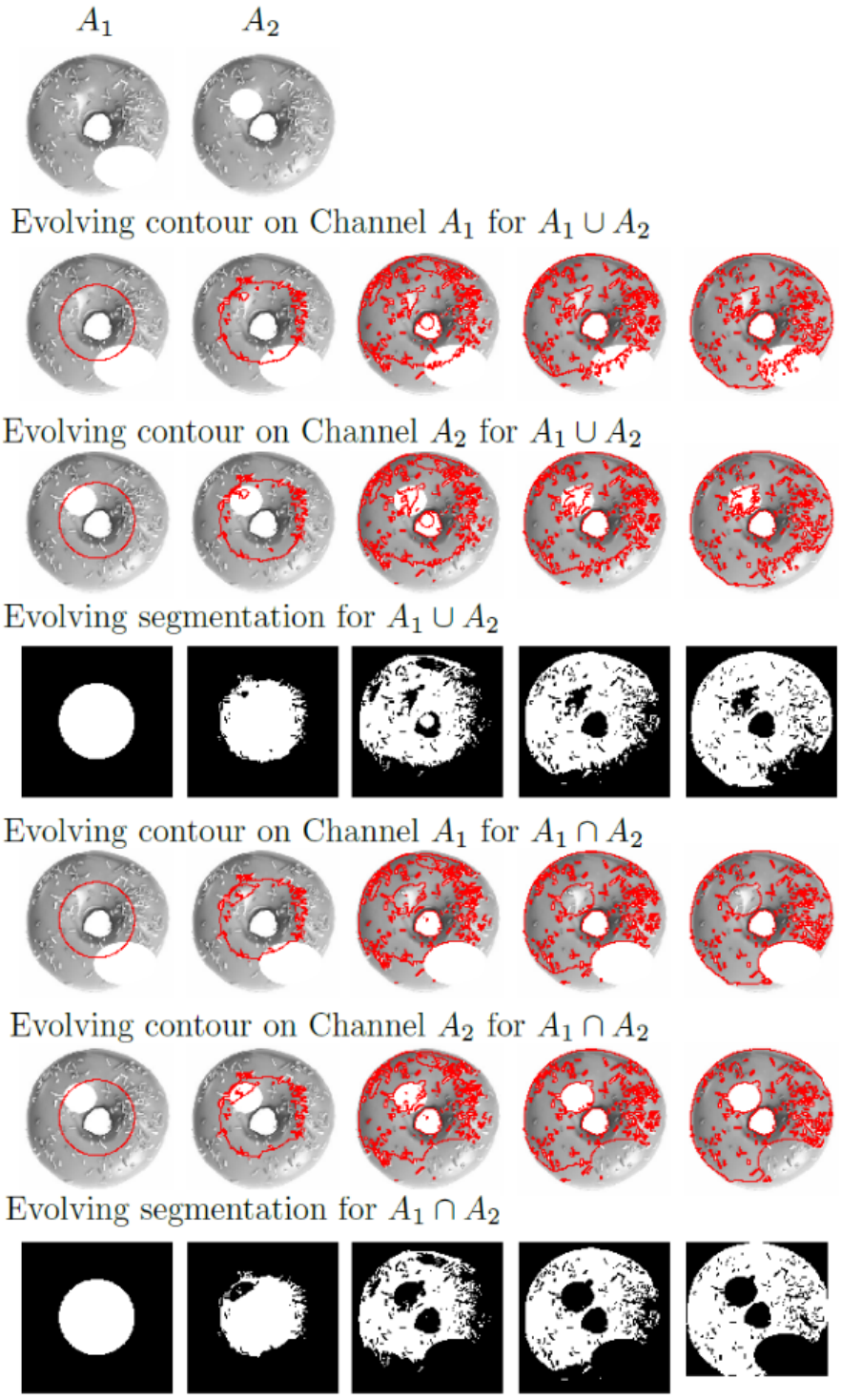


Figure 18. Performing union and intersection on images with holes. Size = 300 * 300. $\phi_0(x, y) = -\sqrt{(x-150)^2 + (y-150)^2)} + 75$, no reinitialization. For union: cpu = 8.63 sec and iterations = 10. For intersection: cpu = 7.68 sec and iterations = 10.

**Independence of Initial Curve Position**

Similar to the previous model, we needed to ensure that the position of the initial curve does not alter our results. Figure 20 shows the segmentation results obtained for the same image used in Figure 16, but with a different position for the

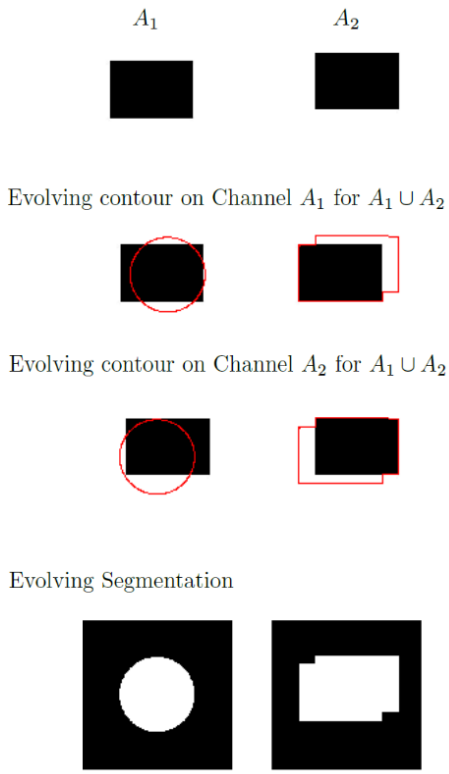


Figure 16. Simple union example. Size = 300 x 300, $\phi_0(x, y) = -\sqrt{(x-150)^2 + (y-150)^2)} + 75$, no reinitialization, cpu = 1.32 s, iterations = 2.

initial curve.

### Reasonable Performance with Blurred Images

Figure 21 shows the union performed on two blurry triangles. We blurred the triangles used in Figure 23, and performed the union operation on them. The full triangle was segmented (the union) despite the blurred edges.

### Reasonable Performance with Noisy Images

To be able to perform well in noisy images, $\lambda$ must be decreased in order to ignore the noise. We added 'Salt & pepper' noise with a variation of 0.1 to the images shown in Figure 24, and tried to perform the union. In the first case shown, we set $\lambda = 255 * 255$ which is the normal setting used for clean images, and in the second case, we set $\lambda = 25$. We show the final segmentation for both cases. In the first case, the noise was detected, while in the second case, the noise was ignored since $\lambda$ was small. This shows that we also satisfy the response to parameter settings criteria since $\lambda$ was the only variation mentioned by the authors in the original paper [5]. We note that the contour evolved much more slowly with a smalled $\lambda$, and thus took much more CPU time, and a larger number of iterations.

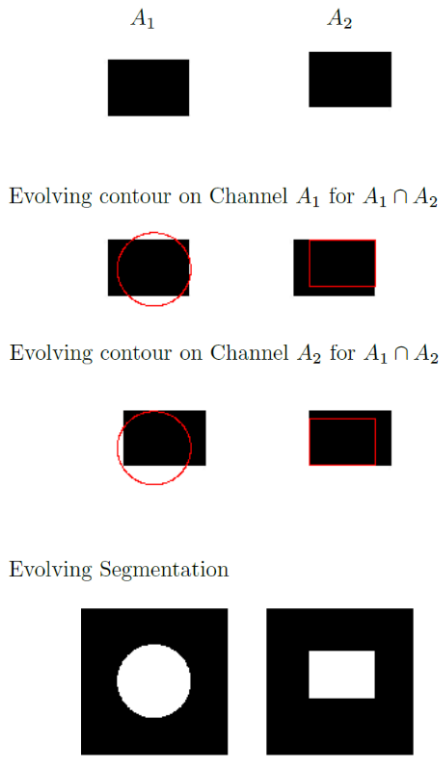


Figure 17. Simple intersection example. Size = 300 x 300, $\phi_0(x, y) = -\sqrt{(x-150)^2 + (y-150)^2)} + 75$, no reinitialization, cpu = 1.83 s, iterations = 2.

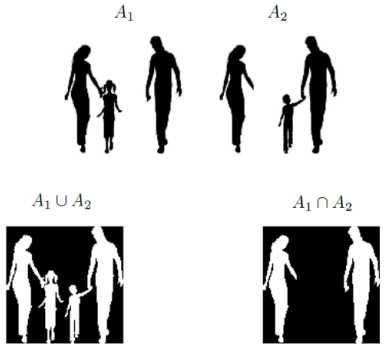


Figure 19. Combining missing information from two different channels. Size = 114 * 114. $\phi_0(x, y) = -\sqrt{(x-57)^2 + (y-57)^2)} + 28.5$, no reinitialization. Union: cpu = 4.01 s and iterations = 7. Intersection: cpu = 4.12 s and iterations = 7.

### Complement

Unfortunately, the complement did not work properly in our implementation. We closely followed the definitions in the original paper where $z_i^{in'} = 1 - z_i^{in}$ and $z_i^{out'} = 1 - z_i^{out}$. The results was actually successfully detected, but continuous flickering occurred, and the curve did not stop in one position. We discuss this results in more details in Section 5.

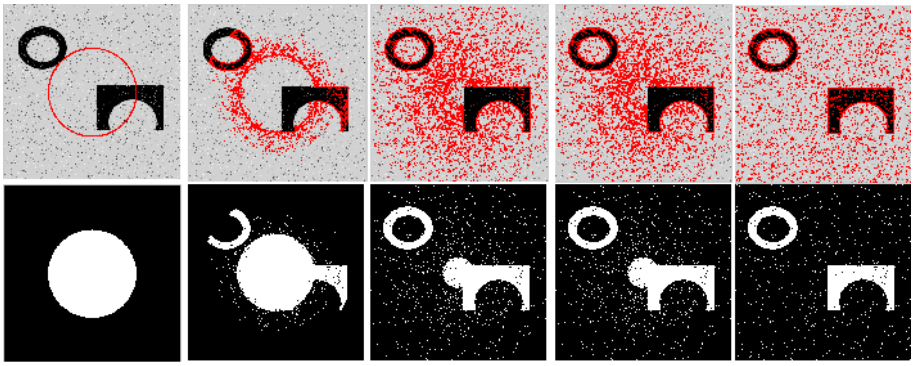

Figure 21. Successful union with blurred images. Top: the evolving curve for $A_1 \cup A_2$ (in red) over time where the first image shows the initial contour. Bottom: evolving segmentation over time until the union is detected. Size = 200 x 200, $\phi_0(x,y) = -\sqrt{(x-100)^2+(y-100)^2)}+50$, no reinitialization, cpu = 6 s, took 11 iterations.

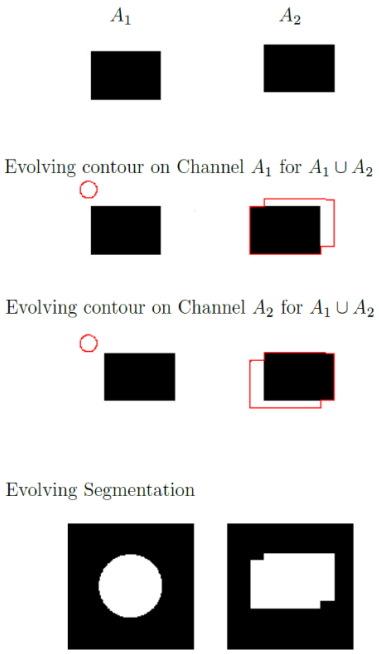


Figure 20. Same example shown in Figure 16, but with different initial curve position. Initial curve does not overlap with either objects. Same segmentation is obtained. Size = 300 x 300, $\phi_0(x,y) = -\sqrt{(x-150)^2+(y-150)^2)}+75$, no reinitialization, cpu = 4.43s, 4 iterations.

### Other Tests

Since the Sandberg-Chan model can successfully detect objects in one channel which are not in another when performing the union, we were curious to know whether this would allow us to perform successful segmentation on colored images by combining the information in the three channels R,G,B. Accordingly, we used the image in Figure 11 which the Chan-Vese model was not able to completely segment. We extracted three channels from the colored image: Red, Green, Black, and performed the union on the three channels. The results are shown in Figure 22. The complete contour of the flowers was successfully detected unlike that obtained in Figure 11.

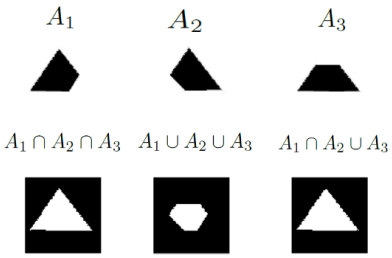


Figure 23. Logic operations performed on three channels. The figure shows the final segmentation in each case. Size = 200 * 200. $\phi_0(x,y) = -\sqrt{(x-100)^2+(y-100)^2)}+50$, $\mu = 0.1$, no reinitialization. For union: cpu = 3.92 sec and iterations = 6. For intersection: cpu = 3.11 sec and iterations = 5. For intersection then union: cpu = 1.24 and iterations = 4.

## 5. Difficulties and Discussion

We have faced many challenges throughout the implementation of this project. Some of the challenges caused major delays in the implementation cycle and hindered us from improving our code and adding more features to it.

### 5.1. Varying mu

$\mu$ is a scaling factor that is used in both the Chan-Vese model and the Sandberg-Chan model to control the weight given to the length of the contour. Therefore, varying the value of $\mu$ will affect the ability to segment objects in noisy images, especially when the noise is similar to Matlab's *salt and pepper* noise. However, varying $\mu$ in our implementation does not really have any impact on the length of the contour. Figure 25 shows the segmentation of an object in a

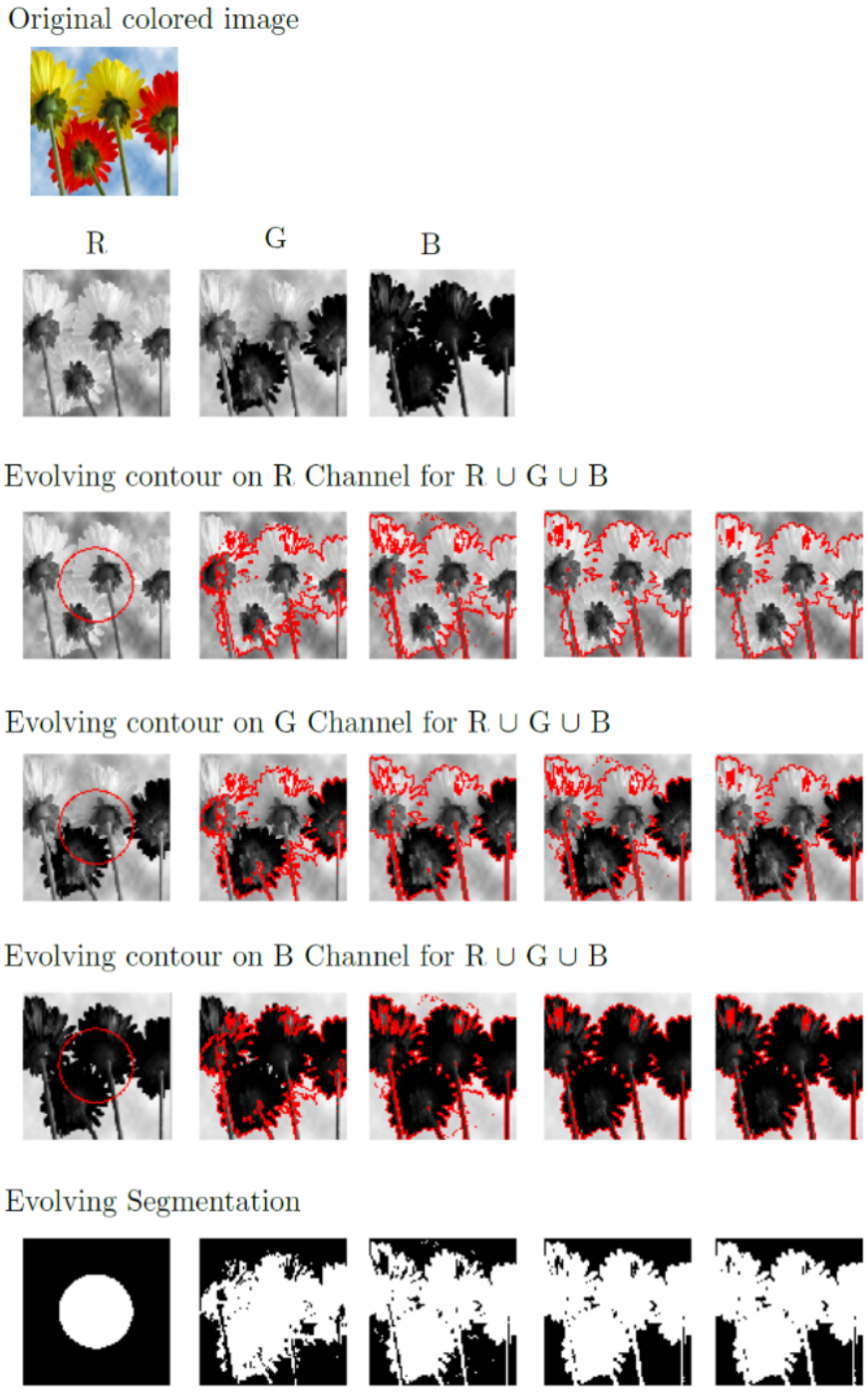


Figure 22. Ability to detect the full contour on a colored image with low variation between foreground and background by taking the union of the RGB channels. Full contour detected as opposed to Figure 11. Size = 300 x 300, $\phi_0(x, y) = -\sqrt{(x - 150)^2 + (y - 150)^2)} + 75$, no reinitialization, size = cpu = 1.73 sec, iterations = 7.

noisy for different values for $\mu$. The resulting segmentation is the same for all values of $\mu$. It is worth noting that this challenge kept us busy for over two days, after which we decided we should move on to other parts of the project.

### 5.2. Computing the complement

The Sandberg-Chan model supports the complement logic operator, so one can segment the logic object ($A \cap \neg B$) (i.e. segment what is in channel A and not in channel B).

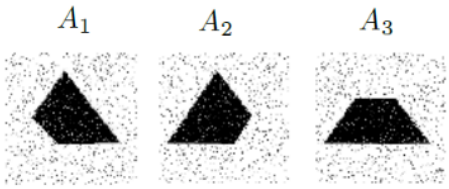


Segmentation for $A_1 \cup A_2 \cup A_3$ with $\lambda = 255 * 255$

Segmentation for $A_1 \cup A_2 \cup A_3$ with $\lambda = 125$

Figure 24. Same image as Figure 23, but with 'salt & pepper' noise with a variation of 0.1. Decreasing $\lambda$ from 255*255 to 125 allowed less noise to be detected. Size = 200 x 200, $\phi_0(x, y) = -\sqrt{(x-100)^2 + (y-100)^2)} + 50$, no reinitialization. Cpu = 3.17 sec and iterations = 5 when $\lambda = 255 * 255$. Cpu = 146.46 sec and iterations = 125 when $\lambda = 125$.

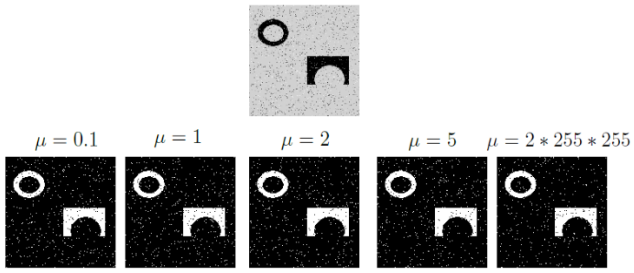


Figure 25. $\mu$ does not have any effect on the length of the contour. *Salt and pepper* noise was added to the original image for testing purposes. Top: original image with noise. Bottom: segmentation for various values of $\mu$.

The model defines the complement of the object in channel *i* as follows:

$$z_i^{in'} = 1 - z_i^{in}, z_i^{out'} = 1 - z_i^{out}. \quad (7)$$

Although the definition is very simple, it does not work in practice. We implemented the complement logic operator as defined in Equation 7, and the segmentation does not stop at the required result. It rather keeps evolving after reaching the required solution, then keeps flipping between two segmentations: the correct segmentation, and the segmentation of $A \cap B$. Figure 26 shows this scenrio. We tried to debug the reasons for this problem for three days.

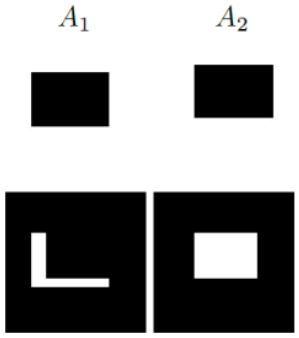


Figure 26. The complement operator causes the contour to go through an infinite loop between two segmentations: the correct segmentation, and the segmentation of $A_1 \cap A_2$. Bottom: correct and incorrect segmentation respectively

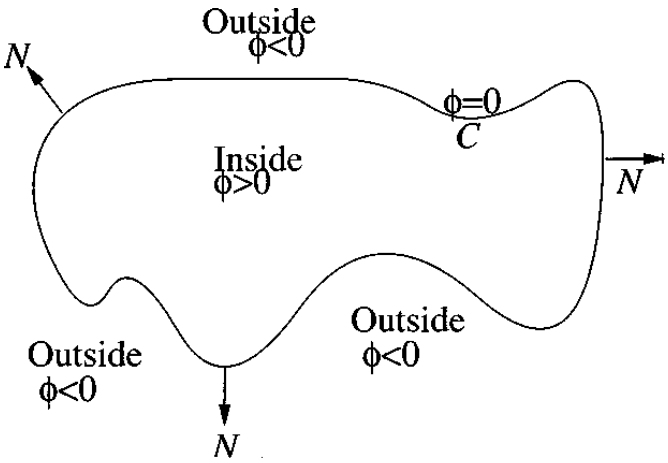


Figure 27. Assumptions about the way $\phi_0$ is defined.

### 5.3. Defining the initial contour phi0

Both the Chan-Vese model and the Sandberg-Chan model defines the initial contour $\phi_0$ as a signed distance function where $\phi_0$ is positive inside the contour $C$, zero on the boundary of $C$ ($\partial C$), and negative outside the contour $C$. Figure 27 illustrates those assumptions.

Since we model our initial contour as a circle, we have to modify the regular equation of the circle to match those assumption. Therefore, we initialize $\phi_0$ as follows:

$$\phi_0(x, y) = radius - \sqrt{(x - c_x)^2 + (y - c_y)^2}, \quad (8)$$

where $c_x$ and $c_y$ are the x-coordinate and y-coordinate of the center of the circle respectively.

Although this definition of $\phi_0$ is compatible with most of the images we used to test our implementation, it did fail to correctly segment the objects in some images. In fact, the results were the opposite of the used logic operator (i.e. the output is the intersection of the channels, while it should

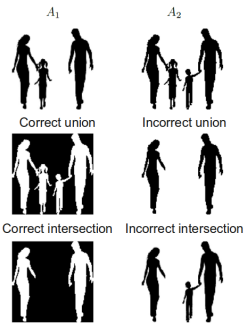


Figure 28.

be the union). After spending quite sometime to resolve this problem and checking what might be the source of the error, we tried using the regular equation of a circle to initialize $\phi_0$ (Equation **??**). We were very intrigued to notice that this modification resulted in the correct segmentation of the input channels. Figure 28 shows the final segmentation using both definitions for $\phi_0$.

$$\phi_0(x, y) = \sqrt{(x - c_x)^2 + (y - c_y)^2} - radius, \qquad (9)$$

where $c_x$ and $c_y$ are the x-coordinate and y-coordinate of the center of the circle respectively.

### 5.4. Mistyped Equations

As previously mentiond in Section 2.2, there is a typo in the equations that define $z_in$ and $z_out$ in the Sandberg-Chan model (equation 3 in thier paper). In addition, they have another typo in the expansion of the the Eular-Lagrange equation for the PDE that models the problem. Both typos consumed over a week of our time until we were able to find out what are the correct equations in both cases. We could have spent this time overcoming other challenges that we faced while implementing both models.

## 6. Conclusion

In this project, we have provided an implementation for the Chan-Vese model for active contours without edges and the Sandberg-Chan logic framework for multi-channel images, both written in Matlab. Our experiments have shown that the Chan-Vese model is effective for various types of images. In specific, it is useful when an edge-based segmentation is not applicable (i.e. edges do not depend on a gradient). However, our implementation fails to respond to different values for the contour length scaling parameter, $\mu$. This affects the ability of our implementation to handle Matlab's *salt & pepper* noise. On the other hand, changing the values for the intensity weight parameters $\lambda_1$ and $\lambda_2$ affects the amount of details obtained inside and outside the segmented object respectively.

We have also shown that our implementation for the Sandberg-Chan logic framework handles different logic combinations for multiple channels. We have also experimented using it as a segmentation tool for colored images by modeling an input colored images as a 3-channel image (red, green, blue). However, our implementation for the *complement* logic operation seems to be missing a hidden trick in the Sandberg-Chan logic framework.

## References

[1] V. Caselles, R. Kimmel, and G. Sapiro. Geodesic active contours. *International journal of computer vision*, 22(1):61–79, 1997.

[2] T. Chan and L. Vese. Active contours without edges. *IEEE Transactions on image processing*, 10(2):266–277, 2001.

[3] M. Kass, A. Witkin, and D. Terzopoulos. Snakes: Active contour models. *International journal of computer vision*, 1(4):321–331, 1988.

[4] D. Mumford and J. Shah. Optimal approximations by piecewise smooth functions and associated variational problems. *Communications on pure and applied mathematics*, 42(5):577–685, 1989.

[5] B. Sandberg and T. Chan. A logic framework for active contours on multi-channel images. *Journal of Visual Communication and Image Representation*, 16(3):333–358, 2005.

[6] G. Sapiro. Color Snakes* 1. *Computer Vision and Image Understanding*, 68(2):247–253, 1997.

[7] S. Zhu and A. Yuille. Region competition: Unifying snakes, region growing, and Bayes/MDL for multiband image segmentation. *Pattern Analysis and Machine Intelligence, IEEE Transactions on*, 18(9):884–900, 2002.